Letter

Magnetic frustration in a van der Waals metal CeSiI

Ryutaro Okuma [1,2,*] Clemens Ritter [3] Gøran J. Nilsen,[4] and Yoshinori Okada[1,†]

[1]*Okinawa Institute of Science and Technology Graduate University, Onna-son, Okinawa 904-0495, Japan*

[2]*Clarendon Laboratory, University of Oxford, Oxford OX1 3PU, United Kingdom*

[3]*Institut Laue-Langevin, 71 Avenue des Martyrs, 38042 Grenoble, France*

[4]*ISIS Neutron and Muon Source, Science and Technology Facilities Council, Didcot OX11 0QX, United Kingdom*

(Received 25 August 2021; revised 16 October 2021; accepted 12 November 2021; published 6 December 2021)

The realization of magnetic frustration in a metallic van der Waals (vdW) coupled material has been sought as a promising platform to explore novel phenomena, both in bulk matter and in exfoliated devices. However, a suitable material realization has been lacking so far. Here, we demonstrate that the vdW compound CeSiI hosts itinerant electrons coexisting with exotic magnetism. In CeSiI, the magnetic cerium atoms form a triangular bilayer structure sandwiched by vdW stacked iodine layers. From resistivity and magnetometry measurements, we confirm the coexistence of itinerant electrons with magnetism with dominant antiferromagnetic exchange between the strongly Ising-like Ce moments below 7 K. Neutron diffraction confirms magnetic order with an incommensurate propagation vector $k \sim (0.28, 0, 0.19)$ at 1.6 K, which points to the importance of further-neighbor magnetic interactions in this system. The presence of a two-step magnetic-field-induced phase transition along the c axis further suggests magnetic frustration in the ground state. Our findings provide a material platform which hosts the coexistence of an itinerant electron and frustrated magnetism in a vdW system, where exotic phenomena arising from the rich interplay between the spin, charge, and lattice in low dimension can be explored.

DOI: 10.1103/PhysRevMaterials.5.L121401

The exploration of novel quantum phenomena in van der Waals (vdW) coupled materials is a promising and rapidly growing field motivated by both fundamental physics interest and, thanks to recent advances in exfoliation technologies, device applications [1–4]. An essential component to accelerate the development of the field is to increase the number of materials that host states whose properties are described by multiple coupled degrees of freedom, such as charge, spin, orbital, and lattice [5]. Among these, a particularly interesting playground for discovering phenomena like these has been identified in systems which manifest an interplay between itinerant electrons and magnetism, and intensive studies have been pursued and reported [6–17]. However, a promising area of this playground which simultaneously remains relatively unexplored is that of vdW materials, where itinerant electrons coexist with low-dimensional and potentially frustrated magnetism. Magnetic frustration can result in noncollinear spin textures and field-induced transitions to exotic quantum phases [18,19]. This includes emergent topologically nontrivial spin textures which lead to couplings between the magnetism and the motion of itinerant electrons [20,21]. Furthermore, noncollinear spin textures can couple to lattice degrees of freedom to produce phenomena such as multiferroicity [22].

Part of the reason why magnetic metallic vdW materials are so scarce is that most vdW materials studied so far have been chalcogenides, which tend to be nonmagnetic. Another important class of materials with vdW structures is the halides. The large ionic radius and small number of chemical bonds of halides leads to low-dimensional vdW bonded structures [24]. While typical transition metal halides [25–28] are low-dimensional Mott insulators, this is not the case for reduced rare-earth halides LnX_2. In rare-earth elements with a strong tendency to stabilize the trivalent state, an electron produced by reduction occupies the outer $5d$ orbital of lanthanide rather than the inner $4f$ orbital and metallicity results [29–31]. Moreover, the finding of giant magnetoresistance and ferromagnetic order above room temperature in GdI_2 motivates us to expect that $4f$ magnetism strongly couples to conduction electrons in rare-earth halide materials [32,33].

The ternary system $LnAI$ (Ln = La, Ce, Pr, Gd. A = Al, Si, Ga, Ge) is a class of materials closely related to the reduced rare-earth halides [34–36]. CeSiI appears as a cleavable material in 2DMatpedia [37], and its crystal structure is depicted in Fig. 1(a). Ce atoms form a triangular bilayer in the ab plane sandwiching a honeycomb net of Si. These blocks are terminated by a vdW-coupled layer of iodine. While its synthesis and crystal structure have been reported previously, its physical properties, especially the effect of frustration and the influence of the Fermi surface on magnetism, have never been investigated. In order to demonstrate CeSiI as a promising host of itinerant electrons with frustrated magnetism, we have synthesized crystalline CeSiI by a high-temperature solid-state reaction [33] in a bulk form [Fig. 1(b)] and performed resistivity, magnetometry, heat capacity, and neutron diffraction measurements [38–44].

*ryutaro.okuma@physics.ox.ac.uk

†yoshinori.okada@oist.jp

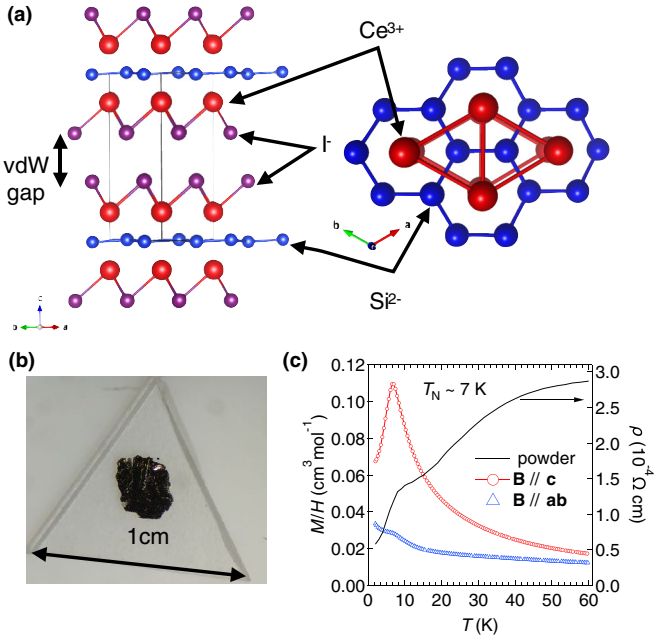

FIG. 1. (a) Crystal structure of CeSiI. Red, blue, and purple spheres indicate Ce, silicon, and iodine atoms, respectively [23]. Red, green, and blue arrows indicate the a, b, and c axes, respectively. (b) Optical microscope image of a single crystal of CeSiI. The image is taken in a globe box filled with pure Ar gas. (c) Temperature dependence of magnetic susceptibilities from a single crystal of CeSiI and zero-field resistivity of a polycrystalline sample of CeSiI. The magnetization measurements were carried out upon cooling in a magnetic field of 1 T applied along the a and c axes.

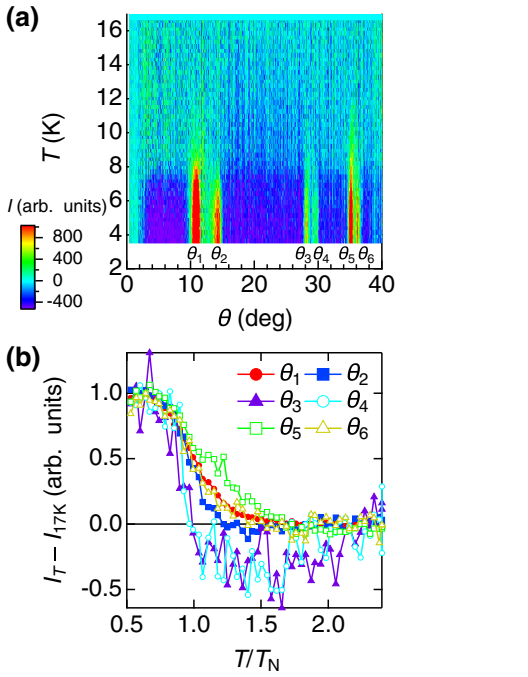

FIG. 2. Neutron diffraction study of CeSiI. (a) Temperature dependence of magnetic diffraction in the temperature range from 16 to 3.8 K. Nuclear reflections were removed from the data by subtracting data obtained at 17 K. The positions of the six observed magnetic Bragg peaks are labeled θ_i (i = 1, . . . , 6). The color scales of the neutron intensity are shown on the right side. (b) The evolution of the integrated intensity around the magnetic Bragg peaks derived from (a). The temperature is scaled by $T_N = 7$ K. The integration intervals for θ_i ($i = 1, \ldots, 6$) are (9.96, 11.56), (13, 14.8), (27.31, 28.5), (28.81, 30.00), (34.13, 35.42), and (35.76, 36.7), respectively. A linear background was assumed in integration.

The coexistence of metallicity and antiferromagnetic interactions in CeSiI is confirmed. Figure 1(c) shows the temperature dependence of the susceptibility $\chi(T)$ along the a and c axes (left axis), together with the temperature dependence of the powder resistivity (right axis). $\chi(T)$ exhibits strongly anisotropic behavior below 100 K due to the trigonal crystalline electric field splitting of the $J = 5/2$ manifold of the Ce^{3+} $4f$ electrons. The lowest Kramers doublet dominates the magnetism below ∼10 K because the other $J = 5/2$ levels are typically located above $10^2 \sim 10^3$ K in the trigonal crystalline electric field [45]. Below 7 K, the susceptibility component along the c axis drops while that along a axis slightly increases, which indicates long-range antiferromagnetic ordering at $T_N \sim 7$ K. The presence of a magnetic phase transition is also confirmed by the drop of resistivity below 7 K due to suppression of electron-spin scattering.

In order to elucidate the magnetic structure, powder neutron diffraction was performed below 20 K on the D20 instrument at ILL [39]. Whereas single-crystal neutron diffraction would be ideal for pinning down the magnetic structure, the required sample volume is difficult to obtain. Nevertheless, as we describe hereafter, powder diffraction still provides essential information to understand this relatively new compound. In Fig. 2(a), we plot the temperature dependence of the low-angle magnetic scattering of CeSiI obtained by subtracting a high-temperature intensity from each 2θ. Six magnetic peaks, which are labeled by $\theta_1 \sim \theta_6$ in Fig. 2(a), are visible below 40° (see Supplemental Material Fig. 3 for the nuclear refinement [38]). As shown in Fig. 2(a), the positions of these peaks are temperature-independent, while their intensity gradually increases below T_N [Fig. 2(b)]. The data quality did not allow for a determination of the critical exponent, however. The increase in the intensity of θ_5 above T_N is affected by a ferromagnetic impurity $CeSi_{1.7}$ with $T_c \sim 14$ K [44]. We note that the change of background below T_N is due to suppression of diffuse scattering from paramagnetic Ce^{3+}. We employed a long scan of the 1.6-K data subtracted by that of the 7.7-K data for the magnetic structure analysis in order to disentangle the effect of diffuse scattering and magnetic Bragg peak.

Indexing the magnetic peaks produced a unique solution with an incommensurate wave vector of $k \sim (0.28, 0, 0.19)$. In the space group $P-3m1$, the identity and mirror perpendicular to b axis render the propagation vector invariant, and these make up the little group G_k. The magnetic representation of a crystallographic site at the $2c$ site $(0, 0, z)$ can be decomposed into the irreducible representation $\Gamma_1 + 2\Gamma_2$, for which the projected basis vectors are listed in Table I. While the Ce site is separated into two orbits $(0, 0, z)$ and $(0, 0, -z)$ in G_k, the symmetry operation that maps k to $-k$ in the full group relates these two; the real and imaginary coefficients of the basis vectors therefore have opposite and same values between the

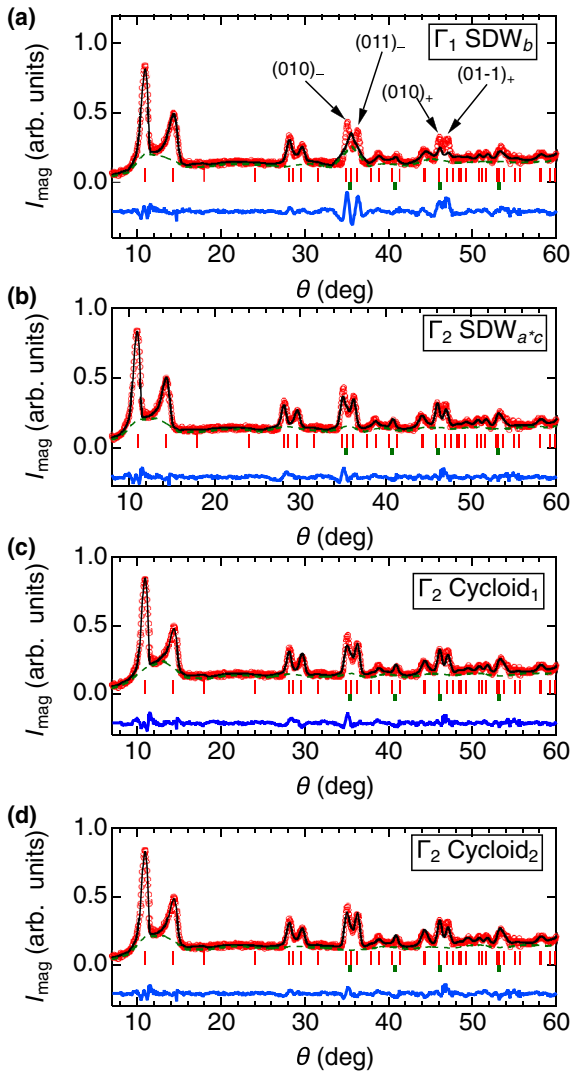

FIG. 3. Powder neutron diffraction pattern of CeSiI and a Rietveld fitting to the magnetic spin structures Γ_1 SDW_b (a), Γ_2 SDW_{a^*c} (b), Γ_2 $Cycloid_1$ (c), and Γ_2 $Cycloid_1$ (d). The red circles represent data taken at 1.6 K after the subtraction of the 7.7-K data as a reference of nuclear contributions. The black, blue, and green line represent a Rietveld fit, a residual of fitting, and background, respectively. The red thin and thick green bar represent the position of magnetic Bragg peaks of CeSiI and $CeSi_{1.8}$ respectively. The arrows indicate the indices of magnetic Bragg peaks, where $(hkl)_{\pm}$ represents a Miller index of $(hkl) \pm q$ reflection, with $q = (0.28, 0, 0.19)$.

two orbits, respectively. Inversion and twofold rotation about the b axis are added to G_k in the full group that also includes time reversal (Supplemental Material, Note 4 [38]).

To determine the magnetic structure below T_N, we refined the neutron diffraction pattern using all possible magnetic structures described by a single irreducible representation: spin-density wave (SDW) along the b axis (SDW_b), which belongs to Γ_1 (in BasIreps notation), and SDW (SDW_{a^*c}) and counter-rotating cycloid ($Cycloid_1$) in the a^*c plane, which belong to Γ_2. $Cycloid_1$ has opposite chiralities between the two orbits to maintain the inversion symmetry. We also consider a structure that breaks sublattice symmetry but

TABLE I. Irreducible representations (IRs) and basis vectors (BVs) for the space group $P-3m1$ with $k = (0.28, 0, 0.19)$. The decomposition of the magnetic structure representation for the site 1 $(0, 0, z)$ is $\Gamma_{mag} = \Gamma_1 + 2\Gamma_2$. The BV components of one orbit along a^*, b, and c are shown by m_x, m_y, and m_z, respectively. The other orbit at site 2 $(0, 0, -z)$ has the same BVs.

IR	BV	m_x	m_y	m_z
Γ_1	ψ_1	0	1	0
Γ_2	ψ_2	1	0	0
	ψ_3	0	0	1

transforms according to the little group and is more common than the counter-rotating cycloid; a corotating cycloid ($Cycloid_2$) in the a^*c plane. In all cases, the impurity phase $CeSi_{1.7}$ is included in all the refinement and we confirmed that the existence of the secondary phase does not have any impact on the main conclusions of this study. Further details of the magnetic structures and fits are described in the Supplemental Material, Note 5 [38]. We plot the results of the Rietveld refinement in Figs. 3(a)–3(d) and Table II. As shown in Fig. 3(a), SDW_b is clearly excluded from the candidate magnetic structure because of the poor agreement around the $(010)_-$, $(011)_-$, $(011)_+$, and $(01-1)_+$ reflections. By contrast, SDW_{a^*c}, $Cycloid_1$, and $Cycloid_2$ reproduce the overall behavior of the observed diffraction pattern as indicated

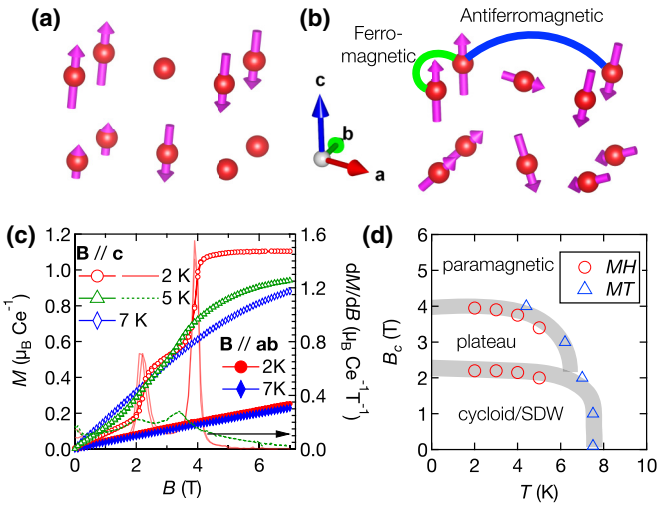

FIG. 4. Magnetic frustration in CeSiI. (a), (b) Magnetic structures are schematically drawn for the case of $Cycloid_2$ and SDW_{a^*c}. Red spheres and magenta arrows indicate the magnetic Ce ions and their magnetic moments, respectively. Red, green, and blue arrows indicate the a, b, and c axes, respectively. (c) Magnetization process of CeSiI. The red, green, and blue circles and red and blue triangles represent magnetization along the c axis at 2, 5, and 7 K and along the ab plane at 2 and 7 K. respectively. The red dotted line is a derivative of magnetization at 2 K, where the peaks indicate the two-step metamagnetic transition. (d) Schematic image of the phase diagram as a function of temperature and magnetic field along the c axis. Open circle and triangle represent transition fields and temperatures determined from the susceptibility and magnetization process, respectively. The shaded regions are eye guides of the phase boundary. See Supplemental Material Fig. 1 for the raw data [38].

TABLE II. Results of Rietveld refinement of neutron diffraction pattern. The magnetic structure models are described in the main text. $m_{i,j}$ represents the component of site j along direction $i = x, y, z$ and $j = 1, 2$. R_p, R_{wp}, and χ^2 represent profile factor, weighted profile factor, and reduced χ^2, respectively.

Model	IR	$m_{x,1}$	$m_{y,1}$	$m_{z,1}$	$m_{x,2}$	$m_{y,2}$	$m_{z,2}$	R_p (%)	R_{wp} (%)	χ^2
SDW_b	Γ_1	0	1.00(1)	0	0	1.00(1)	0	39.2	28.8	6.15
SDW_{a^*c}	Γ_2	0.14(1)	0	1.08(1)	0.14(1)	0	1.08(1)	26.9	18.2	2.59
$Cycloid_1$	Γ_2	0.07(2)i	0	1.11(1)	0.07(2)i	0	–1.11(1)	26.7	18.6	2.76
$Cycloid_2$	Γ_2	0.71(2)i	0	1.024(9)	0.71(2)i	0	1.024(9)	21.8	15.9	2.26

by Figs. 3(b)–3(d) . Thus, based on diffraction experiments, we confirm that a common feature of these three magnetic structures, all of which belong to Γ_2, are a dominant out-of-plane component of the order of 1.0–1.1μ_B. Two of the magnetic structures that yielded the smallest R factors are schematically shown in Figs. 4(a) and 4(b) as representatives of possible magnetic structures, with and without relatively large in-plane magnetic moment.

Finally, we point out that the magnetization process is consistent with the presence of magnetic frustration. Figure 4(c) shows the magnetization process along the out-of-plane ($||c$) and in-plane ($||ab$) directions. Above 4 T the magnetization along the c axis reaches $\sim 1.1\,\mu_B$, which is close to the expected saturated magnetization of SDW_{a^*c} and the $Cycloid_2$ model and suggests the localized nature of the Ce $4f$ moment. The magnetization along the a axis does not saturate below 7 T because this is the hard axis. The key feature is seen at 2 K for the out-of-plane ($//c$) case. Between magnetic fields of 2 T and 4 T, two metamagnetic transitions are clearly observed. The phase diagram as a function of magnetic field along the c axis and temperature is presented in Fig. 4(d). These anomalies are only visible below T_N and are therefore thought to be associated with the magnetic order. It is important to note that the anomalous behavior should be distinct from a simple spin-flop transition in a collinear antiferromagnet, which is usually a single-step process. A similar magnetization process with multiple steps is seen in a number of metallic systems with localized spins such as CeSb [46] and $SrCo_6O_{11}$ [47], of which behaviors are understood as a result of complex spatial dependence of Ruderman-Kittel-Kasuya-Yosida (RKKY) interaction. Given that the $4f$ orbital in cerium atoms are well localized, RKKY interaction accounts for the magnetic order and the field-induced transition. If we turn our attention to layered triangular systems, insulating transition metal iodides are known by similar metamagnetism due to competing nearest-neighbor and further-neighbor coupling. The frustration in interaction leads to a helical order with in-plane periodicity of $(a, 0)$ [48–52], which is analogous to the $Cycloid_2$ case (see Table II). While the origin of magnetic interaction is different between the metallic systems and the insulating ones, the spatial dependence of the magnetic interaction between the spins would be similar. As far as we recognize, the observation of a multiple magnetization process in a vdW metal is a first report in CeSiI.

Our experimental findings collectively point towards CeSiI being a material platform hosting magnetic frustration coexisting with itinerant electrons within a vdW material family. In the case of the out-of-plane SDW [Fig. 4(a)], the realization of a quantum disordered state by frustration and reduced dimensionality will be an interesting question to be explored with the help of the exfoliation technique. Further exotic phases can be expected in the case of the corotating cycloid case [Fig. 4(b)]. For example, the point group of this structure is $m1'$, which allows a finite electric polarization perpendicular to the b axis. Even if polarization is allowed by symmetry, the conduction electrons are expected to screen polarization in metallic compounds. However, in the van der Waals metal WTe_2, which features a polar-nonpolar structural transition, an out-of-plane electric field can switch the displacement of W when atomically thin flakes are used [53].

In summary, we investigated CeSiI using resistivity, magnetometry measurements, and neutron diffraction experiments on both powder and single-crystal samples. Through these we demonstrated that CeSiI is a material platform which searches exotic phenomena arising from the rich interplay between spin, charge, and lattice degree of freedom, for example, by using exfoliation-based device fabrication techniques.

We thank Takeshi Yajima and Hajime Ishikawa for advice on the synthesis of CeSiI, Dmitry Khalyavin for help with the determination of the magnetic structure, and Rieko Ishii, Daichi Ueta, and Wonjong Lee for helping the experiments. This work was carried out by joint research in the Institute for Solid State Physics, the University of Tokyo. R.O. acknowledges support from the European Research Council under the European Union Horizon 2020 Research and Innovation Programme via Grant Agreement No. 788814-EQFT.

[1] K. Geim and I. V. Grigorieva, Van der Waals heterostructures, Nature (London) **499**, 419 (2013).

[2] K. S. Burch, D. Mandrus, and J.-G. Park, Magnetism in two-dimensional van der Waals materials, Nature (London) **563**, 47 (2018).

[3] C. Gong and X. Zhang, Two-dimensional magnetic crystals and emergent heterostructure devices, Science **363**, eaav4450 (2019).

[4] H. Li, S. Ruan, and Y. J. Zeng, Intrinsic van der Waals magnetic materials from bulk to the 2D limit: New frontiers of spintronics, Adv. Mater. **31**, 1900065 (2019).

[5] M. Imada, A. Fujimori, and Y. Tokura, Metal-insulator transitions, Rev. Mod. Phys. **70**, 1039 (1998).

[6] B. Keimer, S. A. Kivelson, M. R. Norman, S. Uchida, and J. Zaanen, From quantum matter to high-temperature superconductivity in copper oxides, Nature (London) **518**, 179 (2015).

[7] G. R. Stewart, Superconductivity in iron compounds, Rev. Mod. Phys. **83**, 1589 (2011).

[8] G. R. Stewart, Heavy-fermion systems, Rev. Mod. Phys. **56**, 755 (1984).

[9] Y. Tokura, K. Yasuda, and A. Tsukazaki, Magnetic topological insulators, Nat. Rev. Phys. **1**, 126 (2019).

[10] Y. Zhang, H. Lu, X. Zhu, S. Tan, W. Feng, Q. Liu, W. Zhang, Q. Chen, Y. Liu, X. Luo, D. Xie, L. Luo, Z. Zhang, and X. Lai, Emergence of Kondo lattice behavior in a van der Waals itinerant ferromagnet, Fe_3GeTe_2, Sci. Adv. **4**, eaao6791 (2018).

[11] Z. Fei, B. Huang, P. Malinowski, W. Wang, T. Song, J. Sanchez, W. Yao, D. Xiao, X. Zhu, A. F. May, W. Wu, D. H. Cobden, J.-H. Chu, and X. Xu, Two-dimensional itinerant ferromagnetism in atomically thin Fe_3GeTe_2, Nat. Mater. **17**, 778 (2018).

[12] K. Kim, J. Seo, E. Lee, K.-T. Ko, B. S. Kim, B. G. Jang, J. M. Ok, J. Lee, Y. J. Jo, W. Kang, J. H. Shim, C. Kim, H. W. Yeom, B. I. Min, B.-J. Yang, and J. S. Kim, Large anomalous Hall current induced by topological nodal lines in a ferromagnetic van der Waals semimetal, Nat. Mater. **17**, 794 (2018).

[13] Y. Deng, Y. Yu, Y. Song, J. Zhang, N. Z. Wang, Z. Sun, Y. Yi, Y. Z. Wu, S. Wu, J. Zhu, J. Wang, X. H. Chen, and Y. Z. Deng, Gate-tunable room-temperature ferromagnetism in two-dimensional Fe_3GeTe_2, Nature (London) **563**, 94 (2018).

[14] J. Li, Y. Li, S. Du, Z. Wang, B.-L. Gu, S.-C. Zhang, K. He, W. Duan, and Y. Xu, Intrinsic magnetic topological insulators in van der Waals layered $MnBi_2Te_4$-family materials, Sci. Adv. **5**, eaaw5685 (2019).

[15] Y. Deng, Y. Yu, M. Z. Shi, Z. Guo, Z. Xu, J. Wang, X. H. Chen, and Y. Zhang, Quantum anomalous Hall effect in intrinsic magnetic topological insulator $MnBi_2Te_4$, Science **367**, 895 (2020).

[16] S. Lei, J. Lin, Y. Jia, M. Gray, A. Topp, G. Farahi, S. Klemenz, T. Gao, F. Rodolakis, J. L. McChesney, C. R. Ast, A. Yazdani, K. S. Burch, S. Wu, N. Phuan Ong, and L. M. Schoop, High mobility in a van der Waals layered antiferromagnetic metal, Sci. Adv. **6**, eaay6407 (2020).

[17] R. Okuma, D. Ueta, S. Kuniyoshi, Y. Fujisawa, B. Smith, C. H. Hsu, Y. Inagaki, W. Si, T. Kawae, H. Lin, F. C. Chuang, T. Masuda, R. Kobayashi, and Y. Okada, Fermionic order by disorder in a van der Waals antiferromagnet, Sci. Rep. **10**, 15311 (2020).

[18] S. Nakatsuji, N. Kiyohara, and T. Higo, Large anomalous Hall effect in a non-collinear antiferromagnet at room temperature, Nature (London) **527**, 212 (2015).

[19] R. Okuma, D. Nakamura, T. Okubo, A. Miyake, A. Matsuo, K. Kindo, M. Tokunaga, N. Kawashima, S. Takeyama, and Z. Hiroi, A series of magnon crystals appearing under ultrahigh magnetic fields in a kagomé antiferromagnet, Nat. Commun. **10**, 1229 (2019).

[20] N. Nagaosa and Y. Tokura, Topological properties and dynamics of magnetic skyrmions, Nat. Nanotechnol. **8**, 899 (2013).

[21] T. Kurumaji, T. Nakajima, M. Hirschberger, K. Kikkawa, Y. Yamasaki, H. Sagayama, H. Nakao, Y. Taguchi, T. Arima, and Y. Tokura, Skyrmion lattice with a giant topological Hall effect in a frustrated triangular-lattice magnet, Science **365**, 914 (2019).

[22] H. Katsura, N. Nagaosa, and A. V. Balatsky, Spin Current and Magnetoelectric Effect in Noncollinear Magnets, Phys. Rev. Lett. **95**, 057205 (2005).

[23] K. Momma and F. Izumi, VESTA 3 for three-dimensional visualization of crystal, volumetric and morphology data, J. Appl. Crystallogr. **44**, 1272 (2011).

[24] J. D. Martin, A. M. Dattelbaum, T. A. Thornton, R. M. Sullivan, J. Yang, and M. T. Peachey, Metal halide analogues of chalcogenides: A building block approach to the rational synthesis of solid-state materials, Chem. Mater. **10**, 2699 (1998).

[25] S. Jiang, L. Li, Z. Wang, K. F. Mak, and J. Shan, Controlling magnetism in 2D CrI_3 by electrostatic doping, Nat. Nanotechnol. **13**, 549 (2018).

[26] B. Huang, G. Clark, D. R. Klein, D. MacNeill, E. Navarro-Moratalla, K. L. Seyler, N. Wilson, M. A. McGuire, D. H. Cobden, D. Xiao, W. Yao, P. Jarillo-Herrero, and X. Xu, Electrical control of 2D magnetism in bilayer CrI_3, Nat. Nanotechnol. **13**, 544 (2018).

[27] R. Klein, D. MacNeill, J. L. Lado, D. Soriano, E. Navarro-Moratalla, K. Watanabe, T. Taniguchi, S. Manni, P. Canfield, J. Fernández-Rossier, and P. Jarillo-Herrero, Probing magnetism in 2D van der Waals crystalline insulators via electron tunneling, Science **360**, 1218 (2018).

[28] J. Yan Banerjee, J. Knolle, C. A. Bridges, M. B. Stone, M. D. Lumsden, D. G. Mandrus, D. A. Tennant, R. Moessner, and S. E. Nagler, Neutron scattering in the proximate quantum spin liquid α-$RuCl_3$, Science **356**, 1055 (2017).

[29] J. D. Corbett, R. A. Sallach, and D. A. Lokken, Physical characterization of the metallic LaI_2 and CeI_2 and of the phase $LaI_{2.42}$, Adv. Chem. **71**, 56 (1967).

[30] J. H. Burrow, C. H. Maule, P. Strange, J. N. Tothill, and J. A. Wilson, The electronic conditions in the 5d1 layer-metal LaI_2 making comparison with the iso-electronic tantalum dichalcogenides, with the other RE di-iodides, and with the RE monochalcogenides, J. Phys. C: Solid State **20**, 4115 (1987).

[31] G. Meyer, N. Gerlitzki, and S. Hammerich, Rare-earth diiodides and derivatives, J. Alloy. Comp. **380**, 71 (2004).

[32] P. H. Müller Kasten and M. Schienle, Magnetic ordering in GdI_2, Solid State Commun. **51**, 919 (1984).

[33] K. Ahn Felser, R. K. Kremer, R. Seshadri, and A. Simon, Giant negative magnetoresistance in GdI2: Prediction and realization, J. Solid State Chem. **147**, 19 (1999).

[34] H. Mattausch and A. Simon, Si_6, Si_{14}, and Si_{22} rings in iodide silicides of rare earth metals, Angew. Chem. Int. Ed. **37**, 499 (1998).

[35] H. Mattausch, C. Zheng, M. Ryazanov, and A. Simon, Reduced lanthanum halides with Ge as interstitials: La_2I_2Ge, La_2I_2Ge, La_3Cl_2Ge, La_3Br_2Ge, La_3I_3Ge, La_6I_5Ge, and $La_{7+x}I_{12}Ge$, Z. Anorg. Allg. Chem. **631**, 302 (2005).

[36] M. Lukachuk, C. Zheng, H. Mattausch, R. K. Kremer, A. Simon, and M. G. Banks, $RE_{2+x}I_2M_{2+y}$ (RE = Ce, Gd, Y; M = Al, Ga): Reduced rare earth halides with a hexagonal metal atom network, Z. Naturforsch. B **62**, 633 (2007).

[37] J. Zhou, L. Shen, M. D. Costa, K. A. Persson, S. P. Ong, P. Huck, Y. Lu, X. Ma, Y. Chen, H. Tang, and P. Y. Feng, 2DMatPedia, An open computational database of two-dimensional materials from top-down and bottom-up approaches, Sci. Data **6**, 86 (2019).

[38] See Supplemental Material at http://link.aps.org/supplemental/10.1103/PhysRevMaterials.5.L121401 for details of synthesis, powder magnetometry, nuclear and magnetic structure refinement, and symmetry analysis, which includes Refs. [39–44].

[39] T. C. Hansen, P. F. Henry, H. E. Fischer, J. Torregrossa1, and P. Convert, The D20 instrument at the ILL: A versatile high-intensity two-axis neutron diffractometer, Meas. Sci. Technol. **19**, 034001 (2008).

[40] J. Rodríguez-Carvajal, Recent advances in magnetic structure determination by neutron powder diffraction, Physica B **192**, 55 (1993).

[41] A. S. Wills, A new protocol for the determination of magnetic structures using simulated annealing and representational analysis (SARAh), Physica B: Condens. Matter **276**, 680 (2000).

[42] H. T. Stokes, D. M. Hatch, and B. J. Campbell, ISODISTORT, ISOTROPY Software Suite, iso.byu.edu.

[43] B. J. Campbell, H. T. Stokes, D. E. Tannera, and D. M. Hatcha, ISODISPLACE: An internet tool for exploring structural distortions, J. Appl. Cryst. **39**, 607 (2006).

[44] H. Yashima and T. Satoh, Nonmagnetic-magnetic transition in Ce-Si system, Solid State Commun. **41**, 723 (1982).

[45] J. Banda, B. K. Rai, H. Rosner, E. Morosan, C. Geibel, and M. Brando, Crystalline electric field of Ce in trigonal symmetry: $CeIr_3Ge_7$ as a model case, Phys. Rev. B **98**, 195120 (2018).

[46] J. Rossat-Mignod, P. Burlet, J. Villain, H. Bartholin, Wang Tcheng-Si, D. Florence, and O. Vogt, Phase diagram and magnetic structures of CeSb, Phys. Rev. B **16**, 440 (1977).

[47] T. Matsuda, S. Partzsch, T. Tsuyama, E. Schierle, E. Weschke, J. Geck, T. Saito, S. Ishiwata, Y. Tokura, and H. Wadati, Observation of a Devil's Staircase in the Novel Spin-Valve System $SrCo_6O_{11}$, Phys. Rev. Lett. **114**, 236403 (2015).

[48] J. W. Cable, M. K. Wilkinson, E. O. Wollan, and W. C. Koehler, Neutron diffraction investigation of the magnetic order in MnI2, Phys. Rev. **125**, 1860 (1962).

[49] T. Kurumaji, S. Seki, S. Ishiwata, H. Murakawa, Y. Tokunaga, Y. Kaneko, and Y. Tokura, Magnetic-Field Induced Competition of Two Multiferroic Orders in a Triangular-Lattice Helimagnet MnI_2, Phys. Rev. Lett. **106**, 167206 (2011).

[50] S. R. Kuindersma, J. P. Sanchez, and C. Haas, Magnetic and structural investigations on NiI_2 and CoI_2, Physica B+C **111**, 231 (1981).

[51] T. Kurumaji, S. Seki, S. Ishiwata, H. Murakawa, Y. Kaneko, and Y. Tokura, Magnetoelectric responses induced by domain rearrangement and spin structural change in triangular-lattice helimagnets NiI_2 and CoI_2, Phys. Rev. B **87**, 014429 (2013).

[52] H. Ju, Y. Lee, K.-T. Kim, I. H. Choi, C. J. Roh, S. Son, P. Park, J. H. Kim, T. S. Jung, J. H. Kim, K. H. Kim, J.-G. Park, and J. S. Lee, Possible persistence of multiferroic order down to bilayer limit of van der Waals material NiI_2, Nano Lett. **21**, 5126 (2021).

[53] Z. Fei, W. Zhao, T. A. Palomaki, B. Sun, M. K. Miller, Z. Zhao, J. Yan, X. Xu, and D. H. Cobden, Ferroelectric switching of a two-dimensional metal, Nature (London) **560**, 336 (2018).